

Feasibility study of logic circuits with a spin wave bus

Alexander Khitun¹, Dmitri E Nikonov², Mingqiang Bao¹,
Kosmas Galatsis¹ and Kang L Wang¹

¹ Device Research Laboratory, Electrical Engineering Department, MARCO Focus Center on Functional Engineered Nano Architectonics (FENA), Western Institute of Nanoelectronics (WIN), University of California at Los Angeles, Los Angeles, CA 90095-1594, USA

² Technology and Manufacturing Group, Intel Corporation, Santa Clara, CA 95054, USA

Received 5 July 2007, in final form 11 September 2007

Published 12 October 2007

Online at stacks.iop.org/Nano/18/465202

Abstract

We present a feasibility study of logic circuits utilizing spin waves for information transmission and processing. As an alternative approach to the transistor-based architecture, logic circuits with a spin wave bus do not use charge as an information carrier. In this work we describe the general concept of logic circuits with a spin wave bus and illustrate its performance by numerical simulations based on available experimental data. Theoretical estimates and results of numerical simulations on signal attenuation, signal phase velocity, and the minimum spin wave energy required per bit in the spin bus are obtained. The transport parameters are compared with ones for conventional electronic transmission lines. The spin wave bus is not intended to substitute traditional metal interconnects since it has higher signal attenuation and lower signal propagation speed. The potential value of a spin wave bus is, however, an interface between electronic circuits and integrated spintronics circuits. The logic circuits with a spin wave bus allow us to provide wireless read-in and read-out.

1. Introduction

There is a growing interest in novel nanometer scale devices and architectures to address the shortcomings and drawbacks inherent to the traditional CMOS-based architecture [1]. Spintronics is one of the most prominent approaches in offering an alternative route to the traditional semiconductor electronics. Recent breakthroughs in the experimental study and control of the spin dynamics in semiconductor nanostructures [2–4] opens new possibilities for spin utilization in information processing. There are some intriguing ideas on possible spin-based logic devices [5–8] taking advantage of the additional degree of freedom provided by spin. It will be extremely beneficial in terms of power consumption to avoid the use of electric current in spin-based circuits. As a possible solution, there was proposed the single spin logic architecture, where the interconnection between the spin-based cells is accomplished via exchange coupling [9]. The use of single-electron or single-spin based devices inherently possesses fundamental drawbacks associated with scheme reliability and fabrication tolerance. To overcome these limitations, there was

recently proposed the utilization of spin waves as a collective physical phenomenon for information transmission [10].

A spin wave is a collective oscillation of spins in an ordered spin lattice around the direction of magnetization. The phenomenon is similar to the lattice vibration, where atoms oscillate around their equilibrium position. Potentially, it is possible to use ferromagnetic films as spin conduits of wave propagation, referred to as a spin wave bus (SWB), where the information can be coded into a phase of the spin wave. The key advantage of the SWB is that information transmission is accomplished without an electron transport. Besides, there are other significant advantages: (i) the ability to use superposition of spin waves in the bus to achieve useful logic functionality; (ii) a number of spin waves with different frequencies can be simultaneously transmitted among a number of spin-based devices; (iii) the interaction between spin waves and the outer devices can be done in a wireless manner, via a magnetic field. The excitation of spin waves can be done by the local magnetic field produced by micro- or nano-scale antenna, while the detection of the spin wave is via the inductive voltage produced by propagating spin waves. The concept

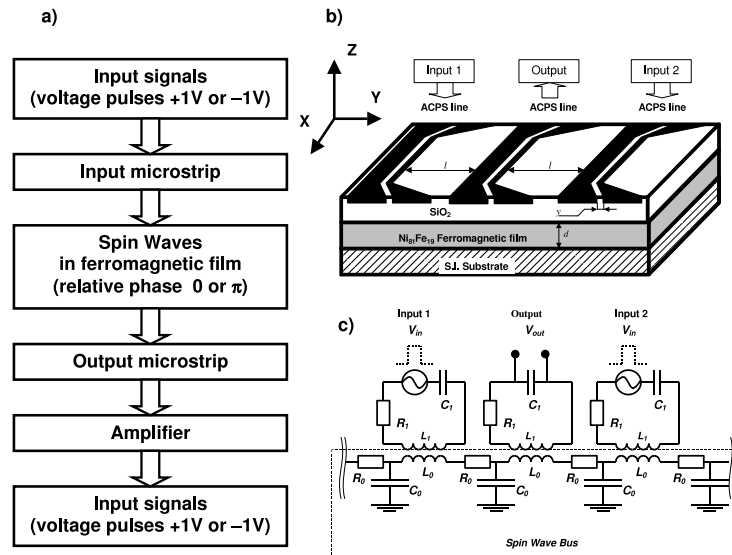


Figure 1. (a) The general concept of logic circuits with SWBs. The operation procedure includes: input signal conversion into the phase of spin wave; data processing using the effect of spin wave superposition; read-out by inductive voltage measurements. (b) An example of a logic circuit with an SWB. Three ACPS transmission lines are made on top of a ferromagnetic layer. The lines and the ferromagnetic layer are isolated by the oxide layer. Each of the ACPS lines can be used for spin wave excitation and detection. Spin waves propagate through the ferromagnetic film, referred to as a 'spin wave bus', and can be detected by the time-resolved inductive voltage measurements. (c) The equivalent circuit consists of the inductively coupled oscillators. The LCR transmission line stands for the spin wave bus.

of a SWB is promising for implementation in different spin-based nano-architectures [10]. An SWB can be utilized as an interface between conventional electronics and integrated magnetic circuits. Specific examples of SWB integration with conventional electron-based devices and spin-based devices are described in [11, 12]. A first working spin wave based logic circuit has been recently experimentally demonstrated [13]. The aim of this work is to offer a different device principle and to provide a more detailed study of the fundamental limitations and shortcomings of the logic circuits with an SWB. One of the most important issues is energy dissipation caused by spin wave damping in the bus, while a low spin wave group velocity is another significant drawback. To understand the transport parameters of the spin bus, we compare them with those for conventional electronic transmission lines. The rest of the paper is organized as follows. In section 2 we describe the general principle of the SWB. In section 3 we consider possible magnetic materials for fabrication and integration of spin waves with conventional silicon platforms. Section 4 is devoted to the spin bus transport characteristics, including signal attenuation and signal phase velocity. In section 5 we analyze power consumption in an SWB; discussions and conclusions are given in sections 6 and 7, respectively.

2. The principle of operation

The general concept of a logic circuit with a spin wave bus is illustrated in figure 1(a). The input data are received in the form of voltage pulses. For simplicity, we assume that input signals of amplitudes +1 and -1 V correspond to the logic states 1 and 0, respectively. Next, the input information is encoded into the phase of the spin wave. The conversion of the voltage signal into the spin wave phase is accomplished by the microstrip antenna. Each microstrip generates a local

magnetic field to excite a spin wave in a ferromagnetic film. Depending on the polarity of the input signal, the initial phase of each spin wave may have a relative phase differences of π . Phases of '0' and ' π ' may be used to represent two logic states 1 and 0. Being excited, spin waves propagate through the spin waveguide or spin wave bus. The data processing in the circuit is accomplished by manipulating the relative phases of the propagating spin waves. The final logic state is detected by the inductive voltage measurement by a receiving microstrip. The sign of the inductive voltage (positive or negative) corresponds to the final logic state. Then, the voltage signal may be amplified by a conventional MOSFET to provide compatibility with the external circuits, after completion of 'computation'.

To illustrate the concept, in figure 1(b) we have shown a prototype logic circuit with two inputs and one output. The core of the structure consists of a ferromagnetic film (NiFe, for example) deposited on an insulating substrate (silicon on insulator (SOI), for example) by a sputtering technique. The film may be entirely polarized along the x -axis when a magnetic field is applied. The thickness of the ferromagnetic layer is on the order of tens of nanometers. There are three asymmetric coplanar (ACPS) transmission strip lines on the top of the structure. These transmission lines are isolated from the ferromagnetic layer by the silicon oxide layer, and are used for spin wave excitation and detection. A voltage pulse applied to an input ACPS line produces a magnetic field perpendicular to the polarization of the ferromagnetic film, and, thus, generates spin waves, and the read-out can be done by the output ACPS line. The structure is similar to one used for the time-resolved measurements of propagating spin waves [14]. In figure 1(c) we show the equivalent circuit for the proposed logic circuit. The input and output circuits consist of the spin-based devices are depicted as LCR oscillators (L_1, C_1, R_1), and the LCR transmission line (L_0, C_0, R_0)

is represented as the spin wave bus. The oscillators are inductively coupled via the interaction with the ferromagnetic film. The film serves as a ‘magnetic’ waveguide transmitting a magnetic field perturbation from one oscillator to another. The change of the current in any of the oscillators produces an inductive voltage in the others, and vice versa. Depending on the relative phase of the currents in the LCR circuits shown in figure 1(c), the resultant inductive voltage at the central circuit can be maximal (in phase) or minimal (out of phase).

An elementary logic gate such as NOT, AND and OR can be realized on the prototype logic circuit shown in figure 1(b). For example, the edge ACPS lines can be considered as the input ports, and the middle ACPS as the output port. The middle ACPS line detects the inductive voltage produced by the *superposition* of two waves. Depending on the relative phase of the spin waves, the amplitude of the inductive voltage may be enhanced (with two waves in phase) or decreased (with two waves out of phase) in comparison to the inductive voltage produced by a single spin wave. The relative phase is defined by the location of the ACPS lines and the polarity of the input excitation voltage signal. It is also possible to control the initial phase by adjusting the time of excitation; with these elementary sets it is possible to realize different logic gates AND, OR, and NOT by controlling the *relative phases* of the spin waves. The detailed numerical simulations show the inductive voltage as a function of the relative phase of two spin waves as given in [10].

3. Spin waveguide materials

Thin film ferromagnetic material is the key element for the proposed spin wave bus circuits. First of all, room temperature operation (high Curie temperature) and long spin relaxation time are important challenges to be overcome. Second, for integration with Si technology, both materials and processing issues need to be addressed. Spin-based devices require both soft and hard metals to produce the desired functionality, and the materials are used in recording (reading) magnetic hard disks. Hard ferromagnetic materials are used to pin (permanent) magnetic orientation, while soft ferromagnetic materials give the ability to change the spin polarization by an external magnetic or electric field. By properly choosing the materials, it is possible to fabricate logic circuits with different logic output. The best polarization obtained for elemental metals has been with Ni and Co, where up to 50% polarization has been obtained [15, 16]. Going beyond elemental metals, alloys such as NiFe have been used. Among these alloys, the most promising metal alloy today for spintronic devices with the highest magnetic moment is $\text{Fe}_{0.65}\text{Co}_{0.35}$ [17].

Recently, in order to achieve the integration with Si electronics and to provide easy electric field control for the next generation of spintronics, a great deal of effort has been devoted to diluted magnetic semiconductors (DMSs). GaN and ZnO have been theoretically shown to possess Curie temperature above room temperature, that is Mn doped [18–20]. For (Ga, Mn)As, experimental results have shown a spin polarization of 85% at 110 K [21]. Nevertheless, II–VI, III–V and group IV are still actively investigated. For all these materials low solubility of Mn and homogeneity are critical limiting factors. Similarly, oxide semiconductors

such as Mn–ZnO [22] and Co–ZnO [23, 24] have also shown promise, and Mn solubility up to 10 mol% at room temperature T_c [25–27]. A review of the literature [27] shows skepticism of ferromagnetism in DMS and oxide semiconductors as ferromagnetism is believed to be induced by insoluble Co, Mn, Ni clusters. In addition, results vary and inconsistent polarization and Curie temperatures are reported [28].

More promising from the perspective of Curie temperatures and spin polarization are half metals. Early theoretical studies indicated that NiMnSb [29] and CrO_2 [30] possess a complete spin split band at the Fermi Level, predicting a polarization of 100%. These predictions have been experimentally confirmed with results coming close to the theoretical maximum [31]. Other half metals include Fe_3O_2 , Heusler metals (such as LSMO [32]), and perovskites (such as $(\text{La}_{1-x}\text{A}_x)\text{MnO}_3$ and $\text{Sr}_2\text{FeMoO}_6$). However, CrO_2 is by far the most researched half metal [31]. A variety of different anti- and ferromagnetic films on silicon have been grown and the exchange integrals of composite materials have also been tabulated [33–36]. Figure 2 shows a summary of popular ferromagnetic materials gaining attention for potential use as spin waveguides.

4. Signal propagation in an LCR line and in a spin wave bus

Signal attenuation and signal group velocity are important parameters to be benchmarked for the spin wave bus. For these parameters, the cross-section dimensions and frequency operation range (from 1 to 100 GHz) of the spin wave bus are the determining factors. In this section we estimate the transport characteristics of the spin transmission line and compare those parameters with these of the conventional electronic transmission line of the same dimension; we give the dimensions in figure 3.

In figure 3(a) we have schematically shown the general and the cross-sectional view of a microstrip line. The line consists of a conductive substrate (ground plane), a dielectric layer and a signal conductor on the top. The dielectric layer has thickness t and relative permittivity ϵ_r , and the signal conductor has thickness d . The signal conductor width is w , and the ground conductor width is g . In figure 3(b) we have shown the general and the cross-sectional view of the spin wave bus. The bus consists of a ferromagnetic wire, which has the same dimensions as the signal conductor. The ferromagnetic film is shown on the top of a non-magnetic insulating substrate. Signal propagation in both cases can be represented as a superposition of two waves traveling in the opposite directions along the copper wire or the ferromagnetic film. The amplitude of the signal can be expressed as follows:

$$A(z, t) = A_1 e^{-\kappa z} \cos(\omega t - \beta z) + A_2 e^{\kappa z} \cos(\omega t + \beta z), \quad (1)$$

where κ represents the attenuation, and β defines the signal velocity $v = \omega/\beta$. These transport parameters let us to compare the performance of two transmission lines regardless of the physical mechanisms of signal propagation.

First, we estimate signal losses in the microstrip transmission line using an LCR model [37]. Here we use the

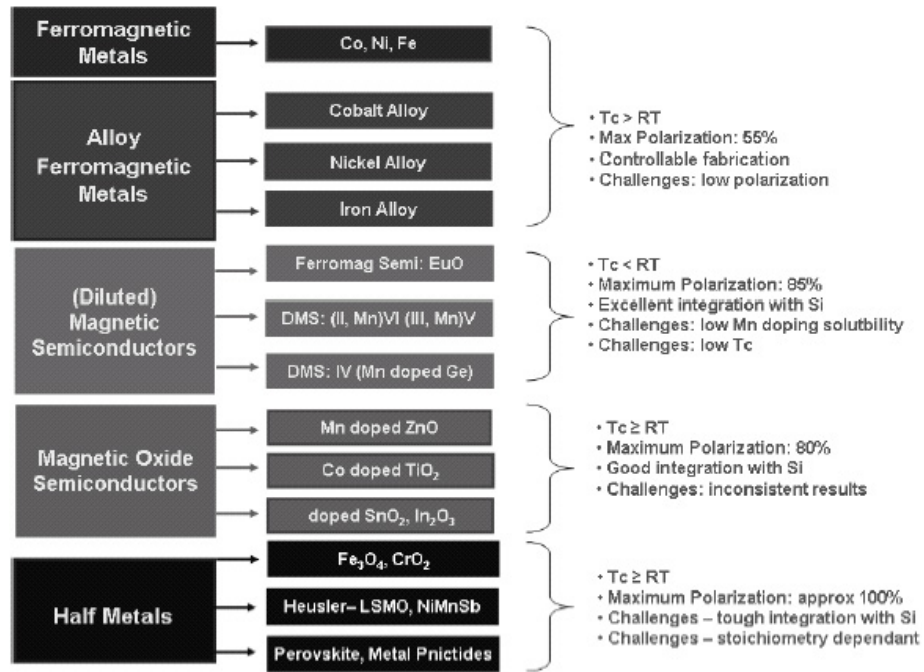


Figure 2. Summary of ferromagnetic materials for potential use as spin waveguides.

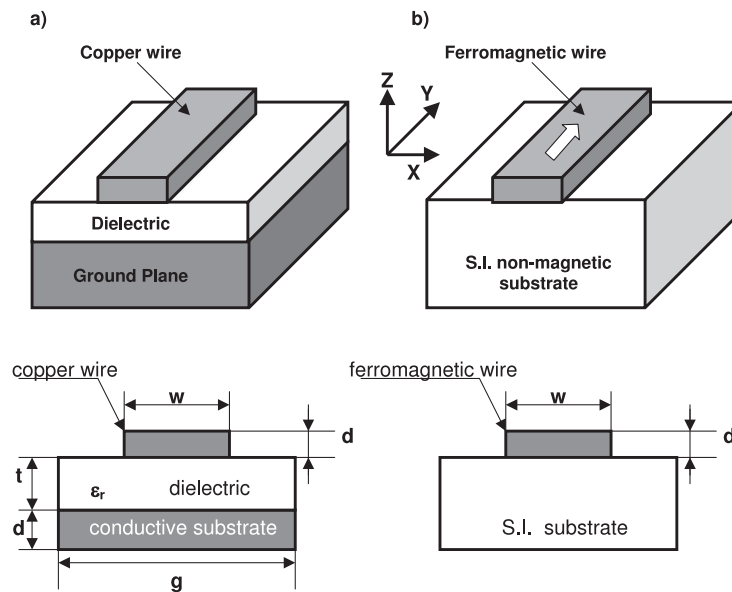


Figure 3. (a) General and cross-sectional view of the microstrip line. From the bottom to the top: conductive substrate of thickness d ; dielectric layer of thickness t and relative permittivity ϵ_r ; signal conductor of thickness d . The signal conductor width is w , and the ground conductor width is g . (b) General and cross-sectional view of the spin wave bus. A ferromagnetic wire is on the top of a non-magnetic insulating substrate. The wire is polarized in the z direction. The wire width is w and the thickness is d .

formula for the transport coefficients given by

$$\kappa = \frac{R}{2} \sqrt{2C/L} \left[1 + \left(1 + \frac{\omega_c^2}{\omega^2} \right)^{1/2} \right]^{-1/2}$$

$$\beta = \omega \sqrt{LC/2} \left[1 + \left(1 + \frac{\omega_c^2}{\omega^2} \right)^{1/2} \right]^{1/2}, \quad (2)$$

where $\omega_c = R/L$, R is the resistance per unit length, L is the inductance per unit length, and C is the capacitance per unit length. At high frequencies the resistance and inductance are subjects of significant modification due to the skin-effect. In order to take the skin-effect into consideration, we use the closed-form formulas found in [38]. Here we reproduce the formula for high-frequency resistance and inductance per unit length [38]:

$$\begin{aligned}
R'(f) &= R'_0 \\
&+ \frac{R'_\infty(f_s) \frac{\sqrt{f/f_s} + \sqrt{1+(f/f_s)^2}}{1 + \sqrt{f/f_s}} - [R'_\infty(f_s) - R'_0]F(f) - R'_0}{1 + \frac{k_r}{1+\omega/h} \log(1 + f_s/f)} \\
L'(f) &= \frac{R'_\infty(f_s) \sqrt{f/f_s}}{2\pi f (1 + \sqrt{f/f_s})} + L'_\infty \\
&+ \left[L'_0 - L'_\infty - \frac{R'_\infty(f_s)}{2\pi f_s} \right] F(f), \quad (3)
\end{aligned}$$

$$F(f) = [1 + (f/f_0)]^{-1/2}, \quad f_0 = \frac{2}{\mu_0} \frac{R_w R_g}{R_w + R_g},$$

$$f_s = \frac{k_s + \frac{10t/w}{1+w/d}}{\pi \mu_0 \sigma t^2},$$

$$R'(0) = R_w + R_g, \quad R_w = \frac{1}{\sigma w t}, \quad R_g = \frac{1}{\sigma g t},$$

where R_w is the resistance per unit length of the signal conductor, R_g is the resistance per unit length of the ground conductor, and $k_s = 1.6$, $k_r = 0.2$ for microstrip lines. The resistance and inductance per unit length in the high-frequency region asymptotically behave as [38]

$$\begin{aligned}
R'(f) &\rightarrow R'_\infty(f) = R'_\infty(f_i) \sqrt{f/f_i} \\
L'(f) &\rightarrow L'_\infty + R'_\infty(f)/\omega, \quad (4)
\end{aligned}$$

where f_i is a chosen (reference) frequency, R'_∞ denotes the skin-effect resistance per unit length, and L'_∞ is the high-frequency external inductance given by $L'_\infty = \frac{\varepsilon_0 \mu_0}{C_0}$, where $\varepsilon_0 = 8.8542 \times 10^{-12}$ F m⁻¹ is the permittivity of vacuum, $\mu_0 = 4\pi \times 10^{-7}$ H m⁻¹ is the vacuum permeability, and C_0 is the transmission line capacitance per unit length in vacuum. The reference skin-effect resistance and inductance were taken for a copper ($\sigma = 56$ MS m⁻¹) microstrip line, $w = 0.2$ mm, $d = 0.1$ mm, $g = 2$ mm, $t = 10$ μ m, at reference frequency 1 GHz: $R'_\infty = 40.64$ Ω m⁻¹, $L'_\infty = 287.6$ nH m⁻¹. The accuracy of the asymptotic formula is estimated to be about 10% [38]. Then, we calculated the losses in the microstrip line in the frequency range from 1 GHz to 1 THz. The results are shown in figure 4. The signal attenuation is of the order of 10³ Np m⁻¹. The losses increase with frequency increase as with scaling down the thickness of the signal conductor. At high frequency ($\omega \gg \omega_c$) the signal velocity approaches its limit—the speed of light in a given dielectric material.

The energy per bit in the metallic interconnect is limited by the Johnson noise

$$V_n = \sqrt{4k_B T Z B_L}, \quad (5)$$

where k_B is the Boltzmann's constant, Z is the line impedance ($Z = \sqrt{\frac{\mu_0}{\varepsilon \varepsilon_0}} = 50$ Ω), the bandwidth of the transmission line B_L must be larger than the inverse rise time τ_n ($B_L > [10\tau_n]^{-1}$), and the intrinsic switching time of a transistor is given by $\tau_n = \frac{C V_{DD}}{I_D}$.

Taking the gate length of 35 nm, and $\tau_n = 2.5$ ps, we obtain that the noise floor is $V_n = 0.18$ mV. Then for 6 dB propagation loss and 3 \times noise margin, the minimum input voltage is $V_{in,met} = 2.2$ mV and the energy per bit at 10 GHz is

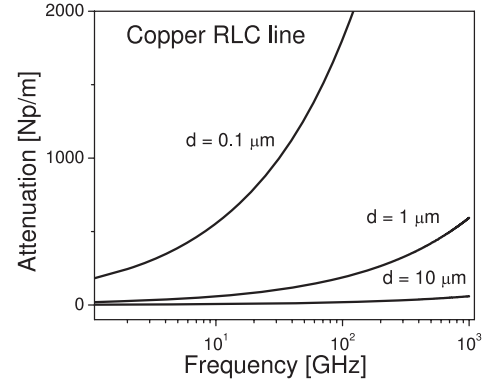


Figure 4. Results of numerical simulations on signal propagation in microstrip line taking into account the skin-effect. Signal attenuation as a function of frequency for different size of the signal conductor 10, 1, and 0.1 μ m.

$E_{met} = 10^{-18}$ J. Even though this limit is proportional to $k_B T$, it is three orders of magnitude larger due to the factors in the noise limit.

Next, we describe the spin wave propagation in a ferromagnetic layer using the Landau–Lifshitz–Gilbert equation:

$$\frac{d\vec{m}}{dt} = -\frac{\gamma}{1 + \alpha^2} \vec{m} \times \left[\vec{H}_{eff} + \alpha \vec{m} \times \vec{H}_{eff} \right], \quad (6)$$

where $\vec{m} = \vec{M}/M_s$ is the unit magnetization vector, M_s is the saturation magnetization, γ is the gyro-magnetic ratio, and α is the phenomenological Gilbert damping coefficient. The first term of equation (6) describes the precession of magnetization about the effective field and the second term describes its dissipation. \vec{H}_{eff} is the effective field given as follows:

$$\vec{H}_{eff} = \vec{H}_d + \frac{2A}{M_s} \nabla^2 \vec{m} + \frac{2K}{M_s} (\vec{m} \cdot \vec{c}) \vec{c} + \vec{H}_{ext}, \quad (7)$$

where $\vec{H}_d = -\nabla\Phi$, $\nabla^2\Phi = 4\pi M_s \nabla \cdot \vec{m}$, A is the exchange constant, K is the uniaxial anisotropy constant, \vec{c} is the unit vector along the uniaxial direction, and \vec{H}_{ext} is the external magnetic field. We restrict our consideration to the magnetostatic waves propagating orthogonally to the film magnetization. In this case we use the analytical formula for spin wave dispersion in a finite-size ferromagnetic film [39] given by

$$\omega = \left[\omega_H (\omega_H + \omega_M) + \frac{\omega_M^2}{4} (1 - e^{-2kd}) \right]^{1/2}, \quad (8)$$

where d is the thickness of the ferromagnetic film, $\omega_H = \gamma H_0$, $\omega_M = \gamma 4\pi M_s$, γ is the gyromagnetic ratio, and H_0 is the external magnetic field at which film magnetization saturates at M_s . The attenuation of the spin waves is due to the magnon–electron, magnon–phonon and magnon–magnon scattering processes. According to the Landau–Lifshitz–Gilbert formalism (equation (6)), the combined effect of all scattering processes is described by the Gilbert damping coefficient α . The decay time τ is given by

$$\tau = (2\pi \gamma \alpha M_s)^{-1}. \quad (9)$$

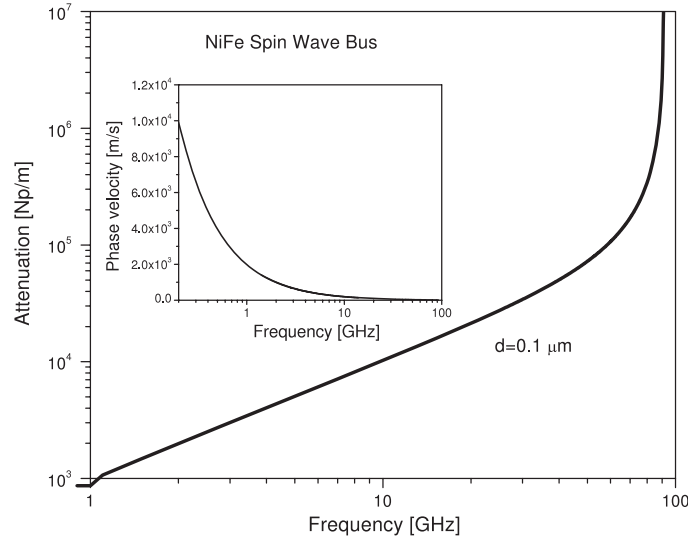


Figure 5. Results of numerical simulations on signal propagation in a NiFe spin wave bus. Signal attenuation as a function of frequency for 0.1 μm thick film. The inset depicts the signal phase velocity as a function of frequency.

We estimate the spin wave attenuation $\kappa = (\tau\nu)^{-1}$ using equations (8) and (9) for 100 nm thick NiFe film. In figure 5 we show the results of numerical simulations showing spin wave attenuation as a function of frequency in the frequency range from 1 to 100 GHz. In our numerical simulations we used the experimentally found Gilbert coefficient $\alpha = 0.0097$ from [14], and the following material characteristics for NiFe: $\gamma = 19.91 \times 10^6 \text{ rad s}^{-1} \text{ Oe}^{-1}$, $4\pi M_s = 10 \text{ kG}$, $H_0 = 200 \text{ Oe}$ taken from the literature [40, 41].

Our estimates show the attenuation of the order of 10^3 Np m^{-1} for GHz region with rapid increase up to 10^7 Np m^{-1} in the high-frequency region 100 GHz. The cause of the losses increase is in the drop of spin wave phase velocity at high frequency. In the inset to figure 5, we depict the phase velocity of the spin wave as a function of wave frequency. The velocity has an order of 10^4 m s^{-1} in the GHz region and exponentially decreases as the frequency increases. The results shown in figure 5 are obtained for specific ferromagnetic material and specific spin wave propagation mode $k \perp H$ (magnetostatic surface spin wave). The phase velocity varies for different ferromagnetic materials and may be increased by applying an external magnetic field or/and modifying the size of the ferromagnetic wire. The fundamental limitation of the spin wave velocity is due to the finite strength of the exchange interaction between the neighbor spins in the lattice. The classical dispersion relation for the spin waves in bulk ferromagnets in the long wavelength limit $ka \ll 1$ (a is the lattice constant) can be rewritten in the following form: $v_p \approx \sqrt{\frac{2\omega Jsa^2}{\hbar}}$, where J is the exchange energy. The higher is the exchange energy the faster are the spin waves in a given ferromagnetic material. For all experimentally studied ferromagnetic materials having high Curie temperature (for example, cobalt and iron having 1388 and 1043 K Curie temperature, respectively,) the spin wave phase velocity does not exceed 10^5 m s^{-1} . Thus, this velocity can be taken as a benchmark for the maximum signal phase velocity in a spin wave bus.

5. Spin wave energy

The spin wave energy E_{sw} can be estimated on very general thermodynamic grounds as follows:

$$E_{\text{sw}} = \mu_0 \Delta M H_{\text{ext}} V, \quad (10)$$

where ΔM is the magnetization change (spin wave amplitude) caused by the external magnetic field of the strength H_{ext} , and V is the material volume. The equation is similar to one presented in [42] for magnetic domain-wall logic, except the magnetization change produced by a spin wave is much less than the saturation magnetization M_s , $\Delta M \ll M_s$. In turn, the amplitude of the external magnetic field required to excite a spin wave is much less than that is required to reverse the magnetization of the whole domain. It is important to recognize a propagating domain wall and a spin wave as two different spin transport mechanisms. A spin wave can be considered a small perturbation of the domain magnetization, and the amplitude of the spin wave can be scaled down with no limit to M_s . The energy of a spin wave may be close to $k_B T$, regardless of the material volume. At the same time, the total energy required to excite the spin wave depends on the efficiency of a given excitation mechanism. As an example, we would like to refer to the spin wave excitation by the local magnetic field generated by microstrips [43]. For a simple geometry (circular loop of radius R), and assuming the distance to the ferromagnetic film to be much less than the antenna radius $d \ll R$, the strength of the magnetic field produced by the antenna is given by

$$H_{\text{ext}} \approx \frac{I_{\text{ext}}}{2\pi R}, \quad (11)$$

where I_{ext} is the excitation current. The strength of the magnetic field required for local magnetization change ΔM , i.e., the amplitude of the spin wave, can be estimated from equation (10) as follows:

$$\frac{\Delta M}{M_s} \approx \gamma \tau_{\text{ext}} H_{\text{ext}}, \quad (12)$$

where τ_{ext} is the duration of the excitation pulse. Using equations (11) and (12), we estimate the energy required for spin wave excitation E_{ext} as follows:

$$E_{\text{ext}} = I_{\text{ext}}^2 \cdot Z \cdot \tau_{\text{ext}} = \left(\frac{\Delta M}{M_s} \right)^2 \left(\frac{2\pi R}{\gamma} \right)^2 \frac{Z}{\tau_{\text{ext}}}, \quad (13)$$

where Z is the impedance. Taking $\Delta M/M_s = 0.01$, $R = 2 \mu\text{m}$, $Z = 50 \Omega$, $\gamma = 19.91 \times 10^6 \text{ rad s}^{-1} \text{ Oe}^{-1}$ ($4.0 \times 10^4 \text{ m A}^{-1} \text{ s}^{-1}$) from [14], and $\tau_{\text{ext}} = 100 \text{ ps}$, we have $E_{\text{ext}} = 4.9 \times 10^{-12} \text{ J}$. For comparison, the spin wave energy obtained for the same parameters using equation (10) is $E_{\text{sw}} = 6.4 \times 10^{-17} \text{ J}$. Only a small part of the excitation energy will be converted into the spin wave energy $E_{\text{sw}} \ll E_{\text{ext}}$. The excitation efficiency can be enhanced by optimizing the antenna structure and prolonging the time of excitation. At any rate, the use of a microstrip antenna is the most convenient but not the optimum way for spin wave excitation.

The most important question is how a small energy spin wave can be detected by the tools of conventional technology. There are several techniques known for spin wave detection: neutron scattering [44], optical measurements [45], magnetoresistance measurements [46] and inductive voltage measurement [41]. We consider time-resolved inductive voltage measurements as the most convenient technique for spin wave detection. According to Faraday's law, the magnitude of the inductive voltage is proportional to the speed of the magnetic flux change $V_{\text{ind}} = -d\Phi/dt$, where Φ is the magnetic flux through the area S of the detecting conducting contour. The sign of the inductive voltage is defined by the rate of the flux change. Thus, two spin waves having π phase difference can be recognized by the sign of the produced inductive voltage. An inductive voltage signal of the order of several mV produced by spin waves propagating through a 27 nm thin ferromagnetic film ($\text{Ni}_{81}\text{Fe}_{19}$) was clearly detected at room temperature [14]. The magnitude of the inductive voltage is proportional to the amplitude of the spin wave, contour area and the spin wave frequency. The peak voltage can be estimated as follows:

$$V_{\text{max}} \approx \mu_0 \Delta M S \omega. \quad (14)$$

Using equations (10) and (14), we plotted in figure 6 the maximum amplitude of the inductive voltage versus the energy of the spin wave in 100 nm thick NiFe film. The amplitude of the inductive voltage can be enhanced by increasing the effective area of the detecting contour (multiple conducting loops), and increasing the spin wave frequency. The spin wave signal has a specific signature—it provides an oscillating output of a certain frequency $V_{\text{in}} \approx V_0 \sin(\omega t)$. By applying a reference signal $V_{\text{ref}} \approx V_1 \sin(\omega t + \theta)$, it is possible to extract the harmonic component in the form of a DC output $V_{\text{DC}} = 0.5 \sqrt{V_0 V_{\text{ref}}} \cos(\theta)$. The current technique, using standard phase lock-in amplifiers, allows us to detect nV (at room temperature). This fact is in favor of spin waves showing the possibility to minimize the operation voltage and decrease power consumption. The use of a lock-in amplifier requires additional energy consumption, and can be implemented efficiently only for final read-out operation.

Magnetoresistance measurements may be an alternative technique for spin wave detection. It was experimentally found

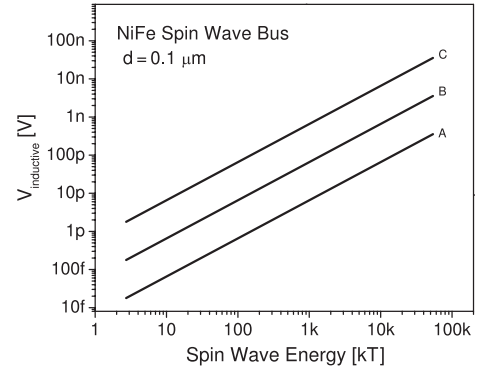


Figure 6. Inductive voltage amplitude as a function of the spin wave energy. Numerical simulations for 100 nm NiFe wire. The lines A, B, and C correspond to the spin wave frequencies 1, 10, and 100 GHz, respectively.

that spin waves play a prominent role in magnetic tunneling junction conductance [46]. The change of the conductance due to the spin waves can be expressed as follows:

$$\Delta \rho_{\text{mag}} \propto \frac{BT}{D(T)^2} \ln \left(\frac{\mu_B B}{k_B T} \right), \quad (15)$$

where B is the inductance, μ_B is the Bohr magneton, and $D(T)$ is the temperature-dependent constant $D(T) = D_0 - D_1 T^2 - D_2 T^{5/2}$, ($D_0 \sim 10^2$, $D_1 \sim 10^{-6}$, $D_2 \sim 10^{-8} \text{ meV A}^2$ at room temperature for Ni film [46]). However, it is not clear whether or not the magnetoresistance measurements can be used for spin wave phase recognition.

6. Discussions

There are many potential advantages for logic circuits with a spin wave bus.

- (i) The local interconnects problem may be resolved, as there are no conducting wires for local interconnection. All communications between the input/output terminals and spin wave bus are via a magnetic field. The coupling occurs in a wireless manner by a magnetic field produced by spin waves.
- (ii) *Enhanced logic functionality.* The utilization of wave superposition offers the possibility to accomplish useful information processing inside the bus, without the use of additional logic elements. A number of logic gates can be realized in one logic circuit.
- (iii) *Parallel data processing.* A number of bits can be encoded in spin waves of different frequencies and processed at constant time.
- (iv) *Defect tolerance.* A new phenomenon of momentum relaxation reversal has been discovered experimentally and explained theoretically for spin waves in ferromagnetic films [47]. It is shown that the process of momentum relaxation, caused by the scattering of a signal wave on defects, can be reversed, and the signal can be self-reconstructed after it has left the scattering region. The reversal of momentum relaxation is achieved by frequency selective parametric amplification of a narrow band of scattered waves having low group velocities and frequencies close to the frequency of the original signal wave. The

effect of momentum relaxation reversal can be used for signal self-correction.

- (v) *Wireless read-in and read-out procedures.* By using micro- or nano-scale antennas it is possible to excite and detect spin waves in a wireless manner.
- (vi) *CMOS compatible processing.* There is no major departure for CMOS fabrication. The layered structure of the device can be easily realized with high accuracy by film deposition by sputtering technique.

A fundamental drawback inherent to the spin wave bus is relatively low spin wave velocity, $\sim 10^5$ m s⁻¹ [14]. The low phase velocity inevitably results in significant time delay for signal propagation. It can be compensated, in part, by taking into account short (of the order of a hundred nanometers) distances among the spin-based devices. Another significant drawback is high signal attenuation. The fundamental cause of spin wave amplitude damping is the scattering on phonons. It has been shown experimentally and verified theoretically that magnetic dissipation plays a significant role in the propagation of spin waves. Due to the dissipation even in high-quality low-loss yttrium iron garnet (YIG) films the propagation length has been found not to exceed 1 cm. The typical spin wave lifetime is limited to the order of a few hundred nanoseconds [48]. We would like to outline that the utilization of spin waves for information transmission may be applicable only for short-range in-chip interconnects which could possibly find suitable use in cellular array-based architectures.

Another important issue is the possibility of obtaining signal gain in a spin wave bus. There are two possible approaches to this problem: (i) amplify the spin wave during propagation in the waveguide, and (ii) amplify the magnetization change produced by the spin wave at the recipient device. To amplify a propagating spin wave perpendicular and parallel microwave pumping can be applied [49]. A possibility to compensate the spin wave's damping and to amplify spin waves propagating in thin ferromagnetic films by parallel pumping has been proven experimentally [50, 51]. A parametric microwave spin wave amplifier giving gain coefficients up to 40 dB for input power levels about 1 pW has been demonstrated experimentally [50]. The use of microwave pumping may not be efficient from a power consumption point of view, as it inevitably results in heat dissipation inside the spin wave bus. It would be more desirable to keep the energy for device-to-device communication minimal and amplify only the final output signal. In other words, it is desirable to amplify the magnetization change caused by the spin wave at the recipient device rather than pump the spin waves in the bus. A possible solution is the combining of a spin wave bus with a diluted magnetic semiconductor (DMS) structure and use the effect of hole-mediated ferromagnetism for signal amplification. In this case, the gain is a function of the DMS cluster size and the critical hole concentration required for the paramagnetic-to-ferromagnetic transition. By estimate, the amplification might be as high as 10^5 – 10^6 at the cost 10^{-17} J for DMS volume 20 nm \times 20 nm \times 100 nm, at the critical hole density 10^{20} cm⁻³.

Cross-talks and capacitive coupling among the transmission lines may be significant with scaling down the separation distance between the excitation/detection ports. The problem of input–output isolation and signal unidirectional propagation is one of the critical design issues for the proposed spin wave based logic devices and it deserves special consideration.

7. Conclusions

We presented a feasibility study of logic circuits with a spin wave bus. The use of spin waves offers an original way to build a wireless nanoscale architecture, where information transmission and processing can be accomplished without a charge transfer. The interaction between the spin wave bus and the other devices is via a magnetic field produced by spin waves. High losses (10^6 Np/m) restrict the potential use of spin waves for information transmission to micrometer range only. Signal propagation in a spin wave bus is limited due to the low group velocity (10^5 m s⁻¹ at most). Energy per bit in the spin wave bus can be scaled down to $1000 k_B T$ at room temperature, limited by the noise factor. However, the efficiency of spin wave excitation by a microstrip antenna is very low, and the energy required for spin wave excitation exceeds the energy of the spin by several orders of magnitude. Signal detection can be accomplished by (i) inductive voltage measurements and (ii) magnetoresistance measurements. Potentially, the use of a spin wave may be the most efficient way for spin-based device interconnection. A set of logic gates can be realized in one module consisting of a number of devices united with a spin wave bus.

Finally, we would like to summarize our conclusions on the spin wave bus.

- A spin wave bus is inferior to traditional metal interconnects in all figures of merit;
- low group velocity limits the signal propagation time and causes significant delay inherent for a spin wave bus;
- spin wave excitation by the electric currents is energetically inefficient;
- logic devices with a spin wave bus requiring a magnetization-to-voltage conversion in each logic element are inferior too;
- the value of a spin wave bus is an interface between electronic circuits and integrated spintronics circuit;
- the logic circuits with a spin wave bus allow us to provide wireless read-in and read-out.

Acknowledgments

We would like to thank Dr G I Bourianoff for insightful discussion. The work was supported in part by the MARCO-FENA center and by the Western Institute of Nanoelectronics.

References

- [1] ITRS, Semiconductor Industry Association 2005 <http://www.itrs.net/Common/2005ITRS/Home2005.htm>
- [2] Ohno H 1998 Making nonmagnetic semiconductors ferromagnetic *Science* **281** 951–6
- [3] Chiba D, Yamanouchi M, Matsukura F and Ohno H 2004 Control of magnetization reversal in ferromagnetic semiconductors by electrical means *J. Phys.: Condens. Matter* **16** S5693–6
- [4] Kato Y K, Myers R C, Gossard A C and Awschalom D D 2004 Observation of the spin Hall effect in semiconductors *Science* **306** 1910–3
- [5] Datta S and Das B 1990 Electronic analog of the electro-optic modulator *Appl. Phys. Lett.* **56** 665–7
- [6] Prinz G A 1998 Magnetoelectronics *Science* **282** 1660–3
- [7] Wolf S A, Awschalom D D, Buhrman R A, Daughton J M, von Molnar S, Roukes M L, Chtchelkanova A Y and

- Treger D M 2001 Spintronics: a spin-based electronics vision for the future *Science* **294** 1488–95
- [8] Nikonov D E and Bourianoff G I 2005 Spin gain transistor in ferromagnetic semiconductors—the semiconductor Bloch-equations approach *IEEE Trans. Nanotechnol.* **4** 206–14
- [9] Bandyopadhyay S, Das B and Miller A E 1994 Supercomputing with spin-polarized single electrons in a quantum coupled architecture *Nanotechnology* **5** 113–33
- [10] Khitun A and Wang K 2005 Nano scale computational architectures with spin wave bus *Superlatt. Microstruct.* **38** 184–200
- [11] Khitun A, Bao M, Lee J-Y, Wang K L, Lee D W, Wang S and Roshchin I V 2007 Inductively coupled circuits with spin wave bus for information processing <http://arxiv.org/ftp/arxiv/papers/0705/0705.3864.pdf>
- [12] Khitun A, Bao M and Wang K L 2007 Spin wave magnetic nanofabric: a new approach to spin-based logic circuitry <http://arxiv.org/ftp/arxiv/papers/0709/0709.0521.pdf>
- [13] Kostylev M P, Serga A A, Schneider T, Leven B and Hillebrands B 2005 Spin-wave logical gates *Appl. Phys. Lett.* **87** 153501
- [14] Covington M, Crawford T M and Parker G J 2002 Time-resolved measurement of propagating spin waves in ferromagnetic thin films *Phys. Rev. Lett.* **89** 237202
- [15] Soulen R J Jr et al 1998 Measuring the spin polarization of a metal with a superconducting point contact *Science* **282** 85–8
- [16] Meservey R and Tedrow P M 1994 Spin-polarized electron tunneling *Phys. Rep.* **238** 173–243
- [17] Johnson D D, Pinski F J and Staunton J B 1987 The Slater–Pauling curve: first principles calculations of the moments of Fe/sub 1-c/Ni/sub c/ and V/sub 1-c/Fe/sub c *J. Appl. Phys.* **61** 3715–7
- [18] Dietl T, Ohno H, Matsukura F, Cibert J and Ferrand D 2000 Zener model description of ferromagnetism in zinc-blende magnetic semiconductors *Science* **287** 1019–22
- [19] Pearton S J et al 2003 Effects of defects and doping on wide band gap ferromagnetic semiconductors *Physica B* **340–342** 39–47
- [20] Yoon S W, Cho S B, We S C, Yoon S, Suh B J, Song H K and Shin Y J 2003 Magnetic properties of ZnO-based diluted magnetic semiconductors *J. Appl. Phys.* **93** 7879–81
- [21] Ohno H 1999 Properties of ferromagnetic III–V semiconductors *J. Magn. Magn. Mater.* **200** 110–29
- [22] Sharma P, Gupta A, Rao K V, Owens F J, Sharma R, Ahuja R, Osorio Guillen J M, Johansson B and Gehring G A 2003 Ferromagnetism above room temperature in bulk and transparent thin films of Mn-doped ZnO *Nat. Mater.* **2** 673–7
- [23] Ueda K, Tabata H and Kawai T 2001 Magnetic and electric properties of transition-metal-doped ZnO films *Appl. Phys. Lett.* **79** 988–90
- [24] Rode K, Anane A, Mattana R, Contour J P, Durand O and LeBourgeois R 2003 Magnetic semiconductors based on cobalt substituted ZnO *J. Appl. Phys.* **93** 7676–8
- [25] Sato K and Katayama-Yoshida H 2002 First principles materials design for semiconductor spintronics *Semicond. Sci. Technol.* **17** 367–76
- [26] Ziese M 2002 Extrinsic magnetotransport phenomena in ferromagnetic oxides *Rep. Prog. Phys.* **65** 143–249
- [27] Prellier W, Fouchet A and Mercey B 2003 Oxide-diluted magnetic semiconductors: a review of the experimental status *J. Phys.: Condens. Matter* **15** R1583–601
- [28] Ohno H 2003 Molecular beam epitaxy and properties of ferromagnetic III–V semiconductors *J. Cryst. Growth* **251** 285–91
- [29] de Groot R A, Mueller F M, van Engen P G and Buschow K H J 1983 New class of materials: half-metallic ferromagnets *Phys. Rev. Lett.* **50** 2024–7
- [30] Goodenough J B 1971 The two components of the crystallographic transition in VO/sub 2 *J. Solid State Chem.* **3** 490–500
- [31] Coey J M D and Venkatesan M 2002 Half-metallic ferromagnetism: example of CrO/sub 2 *J. Appl. Phys.* **91** 8345–50
- [32] Park J H, Vescovo E, Kim H J, Kwon C, Ramesh R and Venkatesan T 1998 Direct evidence for a half-metallic ferromagnet *Nature* **392** 794–6
- [33] Brandl D, Schoppmann C, Tomaschko C, Markl J and Voit H 1994 Preparation of ultrathin ferric oxide layers using Langmuir–Blodgett films *Thin Solid Films* **249** 113–7
- [34] Chizhik A B, Merenkov D N, Gnatchenko S L, Fronc K and Zuberek R 2001 Magneto-optical studies of the H–T phase diagram of an Fe/Si multilayered film *Fiz. Niz. Temp.* **27** 886–95
- [35] Munford M L, Seligman L, Sartorelli M L, Voltolini E, Martins L F O, Schwarzacher W and Pasa A A 2001 Electrodeposition of magnetic thin films of cobalt on silicon *J. Magn. Magn. Mater.* **226–230** 1613–5
- [36] Saftic B, Rasula N, Zinn W and Chevallier J 1982 Molecular beam epitaxy and magnetic properties of EuS films on silicon *J. Magn. Magn. Mater.* **28** 305–12
- [37] Frye R C and Chen H Z 1992 Optimal self-damped lossy transmission line interconnections for multichip modules *IEEE Trans. Circuits Syst. II* **39** 765–71
- [38] Djordjevic A R and Sarkar T K 1994 Closed-form formulas for frequency-dependent resistance and inductance per unit length of microstrip and strip transmission lines *IEEE Trans. Microw. Theory Tech.* **42** 241–8
- [39] Mathieu C, Jorzick J, Frank A, Demokritov S O, Slavin A N, Hillebrands B, Bartenlian B and Chappert C 1998 Lateral quantization of spin waves in micron size magnetic wires *Phys. Rev. Lett.* **81** 3968–71
- [40] Hiebert W K, Stankiewicz A and Freeman M R 1997 Direct observation of magnetic relaxation in a small permalloy disk by time-resolved scanning Kerr microscopy *Phys. Rev. Lett.* **79** 1134–7
- [41] Silva T J, Lee C S, Crawford T M and Rogers C T 1999 Inductive measurement of ultrafast magnetization dynamics in thin-film Permalloy *J. Appl. Phys.* **85** 7849–62
- [42] Allwood D A, Xiong G, Faullkner C C, Atkinson D, Petit D and Cowburn R P 2005 Magnetic domain-wall logic *Science* **309** 1688–92
- [43] Dmitriev V F and Kalinikos B A 1987 Excitation of spin waves in perpendicularly magnetized ferromagnetic films *Z. Tekh. Fiz.* **57** 2212–20
- [44] Mook H A and Nicklow R M 1973 Neutron scattering investigation of the magnetic excitations in iron *Phys. Rev. B* **7** 336–42
- [45] Kolokoltsev O V and Gaidai Yu A 1999 Measurements of angular and spatial characteristics of magnetostatic wave beams by an optical guided-wave probe *J. Magn. Magn. Mater.* **204** 101–19
- [46] Boye S A, Lazor P and Ahuja R 2005 Magnetoresistance and Hall-effect measurements of Ni thin films *J. Appl. Phys.* **97** 83902
- [47] Melkov G A, Kobljanskyj Yu V, Serga A A, Tiberkevich V S and Slavin A N 2001 Reversal of momentum relaxation *Phys. Rev. Lett.* **86** 4918–21
- [48] Kalinikos B A and Kostylev M P 1997 Parametric amplification of spin wave envelope solitons in ferromagnetic films by parallel pumping *IEEE. Trans. Magn.* **33** 3445–7
- [49] L'vov V S 1994 *Wave Turbulence Under Parametric Excitation* (Berlin: Springer)
- [50] Kalinikos B A, Kovaleva M K and Kovshikov N G 1988 *Izobreteniya Otkrytia* **26** 225
- [51] Melkov G A and Sholom S V 1990 Amplification of surface magnetostatic waves by a parametric pump *Z. Tekh. Fiz.* **60** 118–23